

Geometry-Aligned Differential Privacy for Location-Safe Federated Radio Map Construction

Jijia Tian, Wangqian Chen, Junting Chen, Pooi-Yuen Kam

School of Science and Engineering and Future Network Intelligence Institute (FNii)
The Chinese University of Hong Kong, Shenzhen, Guangdong 518172, China

Abstract—Radio maps that describe spatial variations in wireless signal strength are widely used to optimize networks and support aerial platforms. Their construction requires location-labeled signal measurements from distributed users, raising fundamental concerns about location privacy. Even when raw data are kept local, the shared model updates can reveal user locations through their spatial structure, while naive noise injection either fails to hide this leakage or degrades model accuracy. This work analyzes how location leakage arises from gradients in a virtual-environment radio map model and proposes a geometry-aligned Differential Privacy (DP) mechanism with heterogeneous noise tailored to both confuse localization and cover gradient spatial patterns. The approach is theoretically supported with a convergence guarantee linking privacy strength to learning accuracy. Numerical experiments show the approach increases attacker localization error from 30 m to over 180 m, with only 0.2 dB increase in radio map construction error compared to a uniform-noise baseline.

I. INTRODUCTION

Radio maps are models and structured data that capture radio characteristics in a specific geographic environment, and they can play an important role in optimizing the performance of communication networks [1]–[4]. In multiple-input multiple-output (MIMO) communication systems, one may exploit radio maps to organize historical data to assist channel modeling, enhanced MIMO beam tracking, and efficient interference management [5]–[8]. Furthermore, in low-altitude unmanned aerial vehicle (UAV) networks, radio maps provide comprehensive spatial data that enables flight path planning, reliable communication under possible blockage, and joint communication, sensing and safe flight control [9]–[11].

However, it is challenging to construct up-to-date radio maps, because the environment that affects the signal propagation may be slowly varying in time. As a result, it is essential to keep collecting fresh radio measurement data to monitor the propagation environment [12]–[16]. Consequently, a practical remedy is to exploit the *crowd-sourcing* mechanism that motivates a massive number of mobile terminals to measure and report the channel data they observe to the fusion center. However, a conventional crowd-sourcing radio surveying would impose a critical concern on location privacy, where the mobile terminals are required to report their locations as labels of the reported channel measurement data.

Is it possible to hide the location information in data collection for radio map construction? Federated Learning (FL) provides a generic mechanism to train a model distributively and collaboratively without uploading the raw data [17]–[22].

Specifically, the global radio map model is maintained by a central server, and a subset of model parameters are shared among mobile users; the users update the parameters of the local model based on up-to-date local measurement data, and transmit the updated parameters, instead of the raw data, to the central server for model aggregation [23], [24].

However, as radio map models usually contain geographically structured parameter sets [4], [25] or are themselves geographically structured data arrays [12], [16], uploading the model parameters may still expose the location information of the users, although the original measurement data is kept locally. For example, in a joint radio map and environment map construction problem [3], [4], the model parameters consist of the heights of the obstacles in the neighborhood of the users, and therefore, updating these environment parameters can reveal the location information of the users. As a result, both the original measurement data and the intermediate parameters need to be protected.

While conventional FL may pose a potential risk of leaking location information, a DP strategy may be considered, where zero-mean noise is added to the parameters uploaded to the central server. As a result, the location information hidden in the modeled parameters is scrambled; in addition, when there are a large number of users participating in the federated radio map construction, the zero-mean noise in the update from these users can be averaged out at the central server. However, it is still not clear how to control the noise for both protecting the location privacy and not significantly reducing the learning performance of the radio map under FL.

In this paper, we study the issue of protecting the location privacy of the users in collaborative radio map construction, where the users collect radio measurement data locally under a crowd-sourcing mechanism, and collaboratively train a radio map model under the coordination of a central server. This paper is an extended version of [21].¹ We first demonstrate and analyze the location information leakage in the classical FL scheme. Then, we adopt a geometry-aligned DP scheme to protect the location information by adding zero-mean noise to the parameters uploaded to the central server. Specifically, we develop a noise-adding strategy to protect location information from *two* perspectives. First, the spatial distribution of the differential privacy noise is deliberately chosen to follow the geometric structure of the gradient field, rather than being

¹This work was presented in part at the IEEE International Conference on Communications Workshops (ICC Workshops), Denver, CO, USA, 2024.

uniformly random, such that the localization error of the adversary is maximized. Second, the noise parameters are also tuned to hide the spatial pattern of the noise corrupted gradient field to further protect the location information. A regularized objective is developed to achieve the two competing goals in the proposed geometry-aligned DP framework. We derive the convergence proof for the FL algorithm under such DP scheme and reveal the relation between the convergence and the noise upper bound.

To summarize, this paper makes the following contributions:

- We analyze how the location information may leak from the local gradient for a joint radio map and environment sensing problem. Mathematically, we show that the local gradient tends to decrease in magnitude for the environment-related parameters that are spatially distant from the user. This property implies a simple adversary localization strategy from the local gradients.
- We propose a geometry-aligned DP framework that applies heterogeneous noise to individual parameters in the local gradients. The noise levels are dynamically optimized to maximize the localization error of potential adversarial inference attacks, while simultaneously minimizing the spatial variance of the gradient field. The dual objective safeguards the location-specific spatial patterns embedded in the gradients, while preserving their utility for learning.
- We derive a convergence bound for the proposed federated radio map construction framework with geometry-aligned DP protection. The bound quantifies the trade-off between the learning performance of the radio map model and the strength of location privacy protection.
- Numerical experiments on synthetic urban radio map datasets show that the proposed geometry-aligned DP scheme increases the adversary localization rooted mean squared error (RMSE) from about 30m to over 180m, while degrading the radio map reconstruction mean absolute error (MAE) by only about 0.2dB compared with a conventional uniform-noise DP baseline.

Notation. For a function $F(x, y)$, the notation $\nabla F(x; y) \triangleq \frac{\partial}{\partial x} F(x, y)$ denotes the partial derivative of the function F with respect to variable x , with y held as a fixed parameter.

II. SYSTEM MODEL

To easily illustrate the connection between location privacy and radio map construction, we consider a virtual environment embedded radio map model, which has a set of variables that explicitly capture the environment properties. We consider a dense urban environment with N users distributed on the ground and are served by base stations (BSs) deployed either on towers or carried by low-altitude aerial platforms. Note that in such an environment, it is highly possible that the link between the BS and mobile user is blocked by buildings and trees, depending on the relative locations of the nodes. This motivates the construction of radio maps to capture the link quality between an arbitrary mobile location $\mathbf{p}_u \in \mathbb{R}^3$ and an arbitrary aerial BS location $\mathbf{p}_d \in \mathbb{R}^3$.

A. A Virtual Environment Embedded Radio Map Model

Denote the communication link $\mathbf{p} = (\mathbf{p}_u, \mathbf{p}_d)$ as the location pair of the ground user at \mathbf{p}_u and the BS at \mathbf{p}_d . A radio map $\gamma(\mathbf{p}; \mathbf{h})$ is defined as a mapping from the location pair \mathbf{p} to the corresponding channel gain γ between the two locations \mathbf{p}_u and \mathbf{p}_d , where \mathbf{h} is the environment parameter.

1) *Segmented Propagation Model:* Conventional statistical channel model predicts the channel gain based on the propagation conditions, which can be modeled based on the environment parameter \mathbf{h} as to be illustrated later. Let the distance between the ground user and the aerial BS communication be $d(\mathbf{p}) = \|\mathbf{p}_u - \mathbf{p}_d\|_2$. Denote \mathcal{D}_0 as the set of location pairs \mathbf{p} where the link between the user and the aerial BS is in line-of-sight (LOS), and \mathcal{D}_1 as the set of location pairs where the link is in non-line-of-sight (NLOS). Thus, the channel gain for LOS conditions is modeled by $\beta_0 + \alpha_0 \log_{10} d(\mathbf{p})$, for $\mathbf{p} \in \mathcal{D}_0$, and for NLOS conditions, it is given by $\beta_1 + \alpha_1 \log_{10} d(\mathbf{p})$, for $\mathbf{p} \in \mathcal{D}_1$. The parameters are to be learned in the radio map construction process.

2) *Virtual Environment Model:* The challenge is to characterize the shape of the propagation regions \mathcal{D}_0 and \mathcal{D}_1 . We adopt an equivalent virtual environment model with a simplified ray-tracing mechanism. The general idea is to introduce virtual obstacles at specific locations, each with an appropriate height to possibly intersect with the direct communication path to model the LOS or NLOS scenario.

Specifically, consider that the area is uniformly divided into M grid cells, where each cell m is possibly occupied by a virtual obstacle with height h_m , $m = 1, 2, \dots, M$, where $h_m = 0$ for no obstacle. Collectively, the heights of all virtual obstacles constitute a virtual obstacle map, which can be represented by $\mathbf{h} \in \mathbb{R}^M$. For a direct link $\mathbf{p} = (\mathbf{p}_u, \mathbf{p}_d)$ between the user and the aerial BS, define $\mathcal{B}(\mathbf{p})$ as the set of grid cells underneath the link, and z_m as the corresponding link height at each cell $m \in \mathcal{B}(\mathbf{p})$. The link is considered to be LOS if $h_m < z_m$ for all $m \in \mathcal{B}(\mathbf{p})$, indicating that none of the virtual obstacles blocks the link. Conversely, NLOS condition occurs if $h_m \geq z_m$ for at least one $m \in \mathcal{B}(\mathbf{p})$, indicating that the link \mathbf{p} is blocked by at least one virtual obstacle. An illustration of the relationship between h_m and z_m is shown in Fig. 1. Thus, the virtual obstacle model embedded in the channel gain model can be expressed as

$$\gamma(\mathbf{p}; \mathbf{h}) = \begin{cases} \beta_0 + \alpha_0 \log_{10} d(\mathbf{p}), & h_m < z_m, \forall m \in \mathcal{B}(\mathbf{p}) \\ \beta_1 + \alpha_1 \log_{10} d(\mathbf{p}), & h_m \geq z_m, \exists m \in \mathcal{B}(\mathbf{p}). \end{cases} \quad (1)$$

3) *Radio Map Model with Smoothed Transition:* However, the segmented function (1) leads to abrupt transitions between LOS and NLOS regions which may not be consistent with the reality. To address this, we propose the use of continuous functions to create a smoother transition between LOS and NLOS. Consequently, the radio map is formulated as

$$\gamma(\mathbf{p}; \mathbf{h}) = (\beta_0 + \alpha_0 \log_{10} d(\mathbf{p}))S(\mathbf{p}; \mathbf{h}) + (\beta_1 + \alpha_1 \log_{10} d(\mathbf{p}))(1 - S(\mathbf{p}; \mathbf{h})) \quad (2)$$

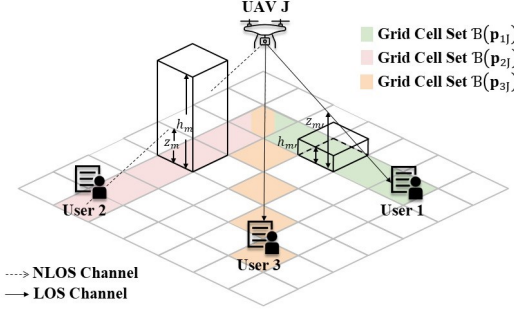


Figure 1. The schematic diagram of virtual obstacle model with the simplified direct communication.

where $S(\mathbf{p}; \mathbf{h})$ is a sigmoid function to approximately model the impact of the LOS and NLOS propagation based on the heights of virtual obstacles \mathbf{h} . Specifically, the function $S(\mathbf{p}; \mathbf{h})$ is defined as

$$S(\mathbf{p}, \mathbf{h}) = \prod_{m \in \mathcal{B}(\mathbf{p})} \psi(z_m(\mathbf{p}) - h_m) \quad (3)$$

where $\psi(x)$ is given by $(1 + e^{-x})^{-1}$. This function represents a logistic function with a smooth transition between 0 and 1. If virtual obstacles in all passing grid cells do not obscure the direct path \mathbf{p} , i.e., $z_m(\mathbf{p}) > h_m, \forall m \in \mathcal{B}(\mathbf{p})$, then $S(\mathbf{p}, \mathbf{h}) \approx 1$ and $\gamma(\mathbf{p}; \mathbf{h})$ approximately equals to the first expression in (1), indicating an LOS scenario; on the other hand, if there exists a virtual obstacle in the passing grid cell that obscures the communication link, i.e., $z_m(\mathbf{p}) < h_m, \exists m \in \mathcal{B}(\mathbf{p})$, then $S(\mathbf{p}, \mathbf{h}) \approx 0$ and $\gamma(\mathbf{p}; \mathbf{h})$ approximately equals to the second expression in (1), indicating an NLOS scenario.

Based on (2), the received signal strength (RSS) from the aerial node \mathbf{p}_d measured at the user location \mathbf{p}_u in a logarithmic scale is formulated as

$$y = \gamma(\mathbf{p}; \mathbf{h}^*) + \xi \quad (4)$$

where ξ captures the randomness due to the residual shadowing and the measurement noise.

B. Radio Map Construction via Federated Learning

Consider a collaborative data collection approach, where each user i collects channel measurements γ following (4) with BSs at various locations. The user-BS location pair dataset collected by user i is denoted by \mathcal{N}_i .

If all the data were available at a central server, the radio map (2) can be constructed by estimating the heights \mathbf{h} and the propagation parameters $\boldsymbol{\theta} = \{\alpha_0, \beta_0, \alpha_1, \beta_1\}$ via minimizing the least-squares cost

$$F(\boldsymbol{\theta}, \mathbf{h}) \triangleq \frac{1}{J} \sum_{i=1}^N \sum_{j \in \mathcal{N}_i} [y_j - \gamma(\mathbf{p}_j; \boldsymbol{\theta}, \mathbf{h})]^2 \quad (5)$$

where \mathbf{p}_j is a sample in the measurement dataset, $J = \sum_{i=1}^N J_i$ denotes the total size of global dataset from all N users, and $J_i = |\mathcal{N}_i|$ denotes the size of i th user dataset \mathcal{N}_i .

We consider a scenario where the measurement data from each user are kept locally and not shared, while FL is used for radio map construction. Specifically, define

$$F_i(\boldsymbol{\theta}, \mathbf{h}) = \frac{1}{J_i} \sum_{j \in \mathcal{N}_i} [y_j - \gamma(\mathbf{p}_j; \boldsymbol{\theta}, \mathbf{h})]^2 \quad (6)$$

as the least-squares cost function of the i th user. The goal cost function (5) relates to the individual cost function as

$$F(\boldsymbol{\theta}, \mathbf{h}) = \sum_{i=1}^N \frac{J_i}{J} F_i(\boldsymbol{\theta}, \mathbf{h}). \quad (7)$$

As illustrated in Fig. 2, the FL radio map construction process consists of the following iterative steps:

- 1) **Broadcasting:** In the t th communication round, the central server broadcasts the current global virtual obstacle map $\mathbf{h}(t)$ and the global propagation parameters $\boldsymbol{\theta}(t)$ to all participating users.
- 2) **Local Training:** Upon receiving the global models, each user i computes the local gradients based on its local dataset \mathcal{N}_i :

- The partial gradient for the environment map \mathbf{h}

$$\nabla F_i(\mathbf{h}(t); \boldsymbol{\theta}) = \frac{1}{J_i} \sum_{j \in \mathcal{N}_i} \nabla [y_j - \gamma(\mathbf{p}_j; \mathbf{h}(t))]^2 \quad (8)$$

- The partial gradient for propagation parameters $\boldsymbol{\theta}$

$$\nabla F_i(\boldsymbol{\theta}(t); \mathbf{h}) = \frac{1}{J_i} \sum_{j \in \mathcal{N}_i} \nabla [y_j - \gamma(\mathbf{p}_j; \boldsymbol{\theta}(t))]^2 \quad (9)$$

- 3) **Model Aggregation:** The central server aggregates the gradients received from N users to update the global environment parameter as

$$\mathbf{h}(t+1) = \mathbf{h}(t) - \eta_h \sum_{i=1}^N \frac{J_i}{J} \nabla F_i(\mathbf{h}(t); \boldsymbol{\theta}) \quad (10)$$

where η_h is the learning rate for \mathbf{h} , and update the global propagation parameter as

$$\boldsymbol{\theta}(t+1) = \boldsymbol{\theta}(t) - \eta_\theta \sum_{i=1}^N \frac{J_i}{J} \nabla F_i(\boldsymbol{\theta}(t); \mathbf{h}) \quad (11)$$

where η_θ is the learning rate for $\boldsymbol{\theta}$.

Under mild assumptions, the FL procedure is guaranteed to converge [26], and the converged solution corresponds to a stationary point of the objective function in (5). However, although FL does not require data sharing, there is still location privacy leakage as analyzed in the next section.

III. POSITION PRIVACY LEAKAGE IN CONVENTIONAL FEDERATED LEARNING

In this section, we analyze how the location information may leak from the local gradient in radio map construction, where we identify an adversary strategy that can infer user location with high precision from the uploaded local gradients.

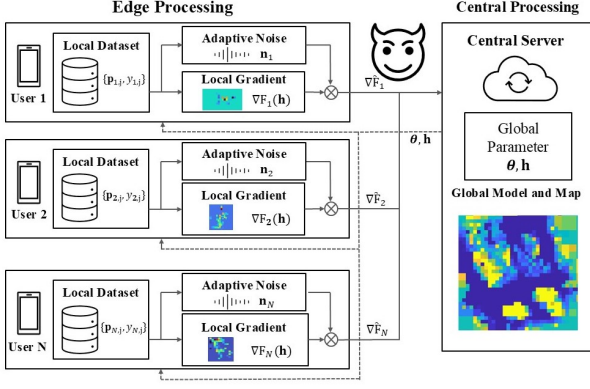


Figure 2. The FL framework for model training: Users calculate local gradients on a locally decomposed model, add artificial noise to the gradient and upload them to the central server for aggregation.

A. Statistics of Local Gradients

It can be shown that the second-order statistics of the local gradient of the environment parameter \mathbf{h} has a strong correlation with the location of the user. Specifically, for the environment parameter h_m that is geographically closer to the user, a larger magnitude of the local gradients is expected.

Let $G_{i,m}$ denote the m th element of the local gradient vector $\nabla F_i(\mathbf{h})$, which represents the gradient contribution with respect to the height h_m of the m th virtual obstacle for user i . From the loss function defined in (6), we can derive the expression for $G_{i,m}$ as

$$G_{i,m} = \frac{2}{J_i} \sum_{j \in \mathcal{N}_i} \Gamma(\mathbf{p}_j; \mathbf{h}) D(\mathbf{p}_j; \mathbf{h}, m) \quad (12)$$

where $\Gamma(\mathbf{p}_j; \mathbf{h})$ is given by

$$\Gamma(\mathbf{p}_j; \mathbf{h}) = (y_j - \gamma(\mathbf{p}_j; \mathbf{h})) \times [(\beta_1 + \alpha_1 \log_{10} d(\mathbf{p}_j)) - (\beta_0 + \alpha_0 \log_{10} d(\mathbf{p}_j))] \quad (13)$$

which captures the model prediction error scaled by the difference between the NLOS and LOS path loss models, and $D(\mathbf{p}_j; \mathbf{h}, m)$ is given by

$$D(\mathbf{p}_j; \mathbf{h}, m) = \frac{\partial}{\partial h_m} S(\mathbf{p}_j; \mathbf{h}) \quad (14)$$

which measures how sensitive the smoothed LOS function $S(\mathbf{p}_j; \mathbf{h})$ is to the change in the height h_m of the specific grid cell m .

In addition, recall that $\mathcal{B}(\mathbf{p}_j)$ represents the collection of grid cells underneath by the communication link \mathbf{p}_j . We define $\mathcal{N}_{i,m} \subseteq \mathcal{N}_i$ to be the subset of user i measurements whose paths traverse cell m , i.e.,

$$\mathcal{N}_{i,m} = \{j | j \in \mathcal{N}_i, m \in \mathcal{B}(\mathbf{p}_j)\}. \quad (15)$$

For the link not above the grid cell m , i.e. $j \notin \mathcal{N}_{i,m}$, the change in the height h_m does not affect the probability

Table I
THE RMSE OF THE PROPOSED ADVERSARY LOCALIZATION STRATEGY

Parameter ν	1	2	5	10	Inf
1st epoch (m)	7.25	6.90	8.26	8.61	9.00
100th epoch (m)	20.69	23.42	17.67	17.23	18.41
200th epoch (m)	27.44	28.93	30.27	30.00	31.44
Average (m)	22.10	24.32	23.52	23.86	24.24

function $S(\mathbf{p}_j; \mathbf{h})$, rendering $D(\mathbf{p}_j; \mathbf{h}, m) = 0$. Thus, the gradient (12) can be expressed as

$$\begin{aligned} G_{i,m} &= \frac{2}{J_i} \sum_{j \in \mathcal{N}_{i,m}} \Gamma(\mathbf{p}_j; \mathbf{h}) D(\mathbf{p}_j; \mathbf{h}, m) \\ &+ \frac{2}{J_i} \sum_{j \notin \mathcal{N}_{i,m}} \Gamma(\mathbf{p}_j; \mathbf{h}) D(\mathbf{p}_j; \mathbf{h}, m) \\ &= \frac{2}{J_i} \sum_{j \in \mathcal{N}_{i,m}} \Gamma(\mathbf{p}_j; \mathbf{h}) D(\mathbf{p}_j; \mathbf{h}, m). \end{aligned} \quad (16)$$

Now we investigate the relationship between the magnitude of $G_{i,m}$ in (16) and the distance away from the i th user. For the i th user at location $\mathbf{p}_{u,i}$, define a subset of grid cells $\mathcal{M}_i = \{m \geq 0 | \mathbf{c}_m = \mathbf{p}_{u,i} + m\boldsymbol{\delta}\}$, representing cells along an arbitrary direction $\boldsymbol{\delta}$ originating from the user. The following result establishes the expected magnitude of the local gradient elements.

Theorem 1 (Gradient Attenuation with Distance). *If $h_m < h_m^*, \forall m \in \mathcal{M}_i$ or $h_m > h_m^*, \forall m \in \mathcal{M}_i$, then, for any $m \in \mathcal{M}_i$ such that $\|\mathbf{c}_{m-1} - \mathbf{p}_{u,i}\| < \|\mathbf{c}_m - \mathbf{p}_{u,i}\|$, the statistics of the corresponding local gradients satisfy*

$$\mathbb{E}\{G_{i,m-1}^2\} \geq \mathbb{E}\{G_{i,m}^2\}. \quad (17)$$

Proof. See Appendix A. \square

Theorem 1 implies that, along any given direction from the user, the expected squared magnitude of the decomposed local gradient $G_{i,m}$ tends to decrease as the distance from the user to the grid cell m increases, provided the estimated obstacle heights h_m along that direction are consistently higher or lower than their true values h_m^* . As a result, an adversary may exploit this property to infer the location of the user.

B. An Adversary Localization Strategy

Inspired by Theorem 1, we demonstrate an adversary strategy to infer the user location based on the local gradients under the FL framework. Specifically, we may adopt a Weighted Centroid Localization (WCL) approach based on the local gradients $G_{i,m}$ as follows.

$$\hat{\mathbf{p}}_{u,i} = \frac{\sum_{m=1}^M |G_{i,m}|^\nu \mathbf{c}_m}{\sum_{m=1}^M |G_{i,m}|^\nu} \quad (18)$$

where \mathbf{c}_m is the coordinate of the m th grid cell, $|G_{i,m}|$ is the magnitude of the local gradient component from user i for cell m , and ν is a positive parameter.

Table I summarizes the location RMSE of the WCL adversary using local gradients obtained at different training epochs. The results show that a localization error below 10 meters can be obtained in the early stages of training, implying a significant privacy risk. This risk is persistent over different parameter settings and training epochs. The most severe leakage occurs in the first epoch, where the adversary achieves a localization error as low as 7–9 meters. This observation directly aligns with Theorem 1, as the training was initialized by $h_m = H_{\max}$, an optimization strategy that was shown to be theoretically desired in previous studies [4]. The accuracy of the adversary strategy degrades as the training process evolves, but an accuracy of less than 30 m can be achieved under $\nu = 1, 2$, implying a significant location privacy leakage for the entire FL training process. This suggests that the gradient remains strongly geographically correlated even beyond the conditions of the Theorem 1.

IV. A REMEDY VIA GEOMETRY-ALIGNED DIFFERENTIAL PRIVACY

In the previous section, it is revealed that the local gradients under the FL framework for radio map construction still contain location information of the user that can be recovered by the central server. The fundamental reason, as illustrated in Theorem 1 based on the radio map model (2), is that some of the model parameters, such as \mathbf{h} in (2), contains environment information and consequently, there may exist some adversary strategies to infer the user location based on the gradients of those environment-related model parameters.

To mitigate the location privacy leakage, we consider a DP approach that adds artificial noise to the local gradient of the obstacle maps $\nabla F_i(\mathbf{h}(t); \boldsymbol{\theta}(t))$ in (8) to obscure the location information implicitly conveyed by the environment-related model parameters. For clarity of discussion, we define the original local gradient of the obstacle map as

$$\mathbf{g}_i(t) \triangleq \nabla F_i(\mathbf{h}(t); \boldsymbol{\theta}(t)). \quad (19)$$

In the DP approach [27], it is first clipped as

$$\bar{\mathbf{g}}_i(t) = \mathbf{g}_i(t) \cdot \min \left(1, \frac{C}{\|\mathbf{g}_i(t)\|_2} \right) \quad (20)$$

to ensure that $\|\bar{\mathbf{g}}_i(t)\|_2 \leq C$, where C is the clipping threshold for bounding $\mathbf{g}_i(t)$. Then noise is added to the clipped local gradient $\bar{\mathbf{g}}_i(t)$ to obtain the uploaded noisy version

$$\tilde{\mathbf{g}}_i(t) = \bar{\mathbf{g}}_i(t) + \mathbf{n}_i(t) \quad (21)$$

where $\mathbf{n}_i(t)$ is zero-mean Gaussian noise $n_{i,m} \sim (0, \sigma_{i,m}^2)$, where the component-wise variance $\sigma_{i,m}^2$ is to be determined later in this section.

To control the overall privacy-utility trade-off, we introduce a design parameter $\mu \geq 0$ that serves as a noise budget. This parameter bounds the total noise variance relative to the signal strength, according to the following condition

$$\mathbb{E}\{\|\mathbf{n}_i(t)\|^2\} \leq \mu \|\bar{\mathbf{g}}_i(t)\|^2. \quad (22)$$

While adding noise deteriorates the convergence of FL, the key challenge here is to strike a balance between learning performance and location privacy protection through controlling

the noise variance $\sigma_{i,m}^2$ under the budget set by μ . In this section, we first establish the convergence of the federated radio map construction under a given noise budget. Then, we develop a mechanism to control the noise variance $\sigma_{i,m}^2$ of different model parameters to maximize location protection.

A. Convergence under Differential Privacy

We first analyze the impact of noise on the FL global objective function $F(\boldsymbol{\theta}, \mathbf{h})$. Existing FL convergence analyses assume identical noise variance. It is not known whether a similar convergence result holds if the distribution of the gradient noise $n_{i,m}$ is not identical.

First, by examining the formulation (2), (3), (5), (7), one can conclude that $F_i(\boldsymbol{\theta}, \mathbf{h})$ and $F(\boldsymbol{\theta}, \mathbf{h})$ are Lipschitz continuous since they are compositions of smooth functions. Denote the Lipschitz constant as L , i.e.,

$$\|\nabla F(\mathbf{x}_1) - \nabla F(\mathbf{x}_2)\| \leq L \|\mathbf{x}_1 - \mathbf{x}_2\| \quad (23)$$

where $\mathbf{x} = (\boldsymbol{\theta}, \mathbf{h})$. We further make the following assumption on the local gradient $\mathbf{g}_i(t) = \nabla F_i(\mathbf{h}(t); \boldsymbol{\theta}(t))$.

Assumption 1 (*B-Local Dissimilarity*). *The local gradient $\mathbf{g}_i(t) = \nabla F_i(\mathbf{h}(t))$ is B-locally dissimilar at a given parameter \mathbf{h} as*

$$\mathbb{E}\{\|\mathbf{g}_i(t)\|^2\} \leq B^2 \mathbb{E}\{\|\mathbf{g}(t)\|^2\} \quad (24)$$

where $\mathbf{g}(t) = \sum_{i=1}^N \frac{J_i}{J} \mathbf{g}_i(t)$ according to (5)–(6), and B is a finite constant that quantifies the degree of deviation between local and global gradients.

This condition holds in our model because the continuous differentiability of our objective function (5) ensures that both local gradients $\mathbf{g}_i(t)$ and the global gradient $\mathbf{g}(t)$ are bounded within any compact set of parameters.

Let $\tilde{J} = \sum_{i=1}^N J_i^2 / J^2$ denote the heterogeneity of the size of the local datasets. From Cauchy-Schwartz inequality, we have $\frac{1}{N} \leq \tilde{J} < 1$, where the lower bound is achieved when $J_1 = J_2 = \dots = J_N$, and \tilde{J} approaches to 1 when J_i are highly heterogeneous.

Lemma 1 (*Global Loss Reduction Bound*). *Given the propagation parameter $\boldsymbol{\theta}(t)$ in each training round, the expected decrease of the loss is bounded as*

$$\mathbb{E}\{F(\mathbf{h}(t+1), \boldsymbol{\theta}(t)) - F(\mathbf{h}(t), \boldsymbol{\theta}(t))\} \leq -\kappa_h \mathbb{E}\{\|\mathbf{g}(t)\|_2^2\} + \kappa_0 \quad (25)$$

where $\kappa_h = \eta_h \left(\frac{1}{2} - \frac{L\eta_h}{2} B^2 (1 + \mu\tilde{J}) \right)$, and $\kappa_0 = \frac{\eta_h B^4 L^4}{8C^2}$.

Given the obstacle map $\mathbf{h}(t+1)$ in each training round, the expected decrease of the loss is bounded as

$$\begin{aligned} \mathbb{E}\{F(\mathbf{h}(t+1), \boldsymbol{\theta}(t+1)) - F(\mathbf{h}(t+1), \boldsymbol{\theta}(t))\} \\ \leq -\kappa_\theta \mathbb{E}\{\|\nabla F(\boldsymbol{\theta}(t); \mathbf{h}(t+1))\|_2^2\} \end{aligned} \quad (26)$$

where $\kappa_\theta = \eta_\theta - \frac{L\eta_\theta^2}{2}$.

Proof. See Appendix B. \square

Combining (25) and (26), the expected decrease of the global function is formulated as

$$\begin{aligned} \mathbb{E}\{F(\mathbf{h}(t+1), \boldsymbol{\theta}(t+1)) - F(\mathbf{h}(t), \boldsymbol{\theta}(t))\} \\ \leq -\kappa_h \mathbb{E}\{\|\mathbf{g}(t)\|_2^2\} + \kappa_0 - \kappa_\theta \mathbb{E}\{\|\nabla F(\boldsymbol{\theta}(t))\|_2^2\}. \end{aligned} \quad (27)$$

By iteratively applying (27) from $t = 0$ to $t = T - 1$, we obtain a bound on the average of the squared gradient norms

$$\begin{aligned} & \frac{1}{T} \sum_{t=0}^{T-1} \kappa (\mathbb{E}\{\|\mathbf{g}(t)\|_2^2\} + \mathbb{E}\{\|\nabla F(\boldsymbol{\theta}(t))\|_2^2\}) \\ & \leq \frac{1}{T} \mathbb{E}\{F(\mathbf{h}(0), \boldsymbol{\theta}(0)) - F(\mathbf{h}(T), \boldsymbol{\theta}(T))\} + \kappa_0 \end{aligned} \quad (28)$$

where $\kappa = \min(\kappa_h, \kappa_\theta)$.

Since the cost function $F(\mathbf{h}, \boldsymbol{\theta})$ is non-negative, as the number of iterations T tends to ∞ , the first term on the right hand side tends to 0. Recall that the total gradient is structured as

$$\nabla F(\mathbf{h}(t), \boldsymbol{\theta}(t)) = [\mathbf{g}(t)^\top, \nabla F(\boldsymbol{\theta}(t))^\top]^\top. \quad (29)$$

As a result, if $\kappa > 0$, we obtain

$$\begin{aligned} & \frac{1}{T} \sum_{t=0}^{T-1} \mathbb{E}\{\|\nabla F(\mathbf{h}(t), \boldsymbol{\theta}(t))\|_2^2\} \\ & \leq \frac{1}{T\kappa} \mathbb{E}\{F(\mathbf{h}(0), \boldsymbol{\theta}(0)) - F(\mathbf{h}(T), \boldsymbol{\theta}(T))\} + \frac{\eta_h B^4 L^4}{8C^2 \kappa} \end{aligned} \quad (30)$$

where the first term tends to 0 as $T \rightarrow \infty$, and the second term is a small number that also tends to zero as the clipping number $C \rightarrow \infty$, i.e., no clipping. Building on this, Corollary 1 provides an upper bound on the expected norm of the total gradient under heterogeneous noise conditions.

Corollary 1 (Convergence under Heterogeneous Noise). *If the learning rate satisfies $0 < \eta_h < \frac{1}{LB^2(1+\mu\tilde{J})}$ and $0 < \eta_\theta < \frac{2}{L}$, then the total gradient is upper bounded by*

$$\lim_{t \rightarrow \infty} \mathbb{E}\{\|\nabla F(\mathbf{h}(t), \boldsymbol{\theta}(t))\|_2\} \leq \sqrt{\frac{\eta_h B^4 L^4}{8C^2 \kappa}} \quad (31)$$

which tends to 0 as the clipping number $C \rightarrow \infty$.

Proof. See Appendix C. \square

Corollary 1 establishes that the federated radio map construction algorithm attains a bounded expected norm for the total gradient, even in the presence of heterogeneous artificial noise added to the local gradients as in (21).

Lemma 1, on the other hand, implies a tradeoff between reducing the expected gradient norm and preserving privacy. Maximizing the descent rate κ_h leads to faster loss reduction with respect to \mathbf{h} . Under this goal, the maximum learning rate for a given noise budget μ is

$$\eta_h^* = \frac{1}{LB^2(1+\mu\tilde{J})} \quad (32)$$

where a larger μ reduces η_h^* , limiting the convergence speed. Conversely, for any fixed learning rate $\eta_h > 0$, ensuring $\kappa_h > 0$ in (27) requires the noise budget to be bounded by

$$\mu < \frac{1}{\tilde{J}} \left(\frac{1}{B^2 L \eta_h} - 1 \right). \quad (33)$$

These expressions quantify the trade-off between privacy and learning performance. A larger noise budget μ improves privacy but reduces the allowable learning rate. As μ increases, both η_h and the descent rate κ_h decrease. This slows the update

of \mathbf{h} and degrades the efficiency of the alternating optimization between \mathbf{h} and $\boldsymbol{\theta}$.

Furthermore, the convergence bound in Corollary 1 includes a residual term controlled by the gradient clipping threshold C , which is introduced to mitigate heterogeneous noise effects. A smaller C improves robustness to noise and strengthens privacy. However, it increases the residual $\sqrt{\frac{\eta_h B^4 L^4}{8C^2 \kappa}}$ leading to a looser convergence bound. In contrast, letting $C \rightarrow \infty$ eliminates the residual but weakens noise control and may reduce privacy protection.

B. Principles of the Geometry-Aligned Differential Privacy

While the total noise budget μ affects the convergence bound as stated in Lemma 1 and Corollary 1, we have the flexibility to distribute the total noise budget μ over individual grid cells $\sigma_{i,m}^2$ to enhance privacy protection without affecting the convergence bound.

Denote $\tilde{G}_{i,m} = \tilde{G}_{i,m} + n_{i,m}$ as the m th element of the noisy gradient element on the i th user. The vector of noise energies across all grid cells is defined as $\boldsymbol{\sigma}_i = (\sigma_{i,1}^2, \dots, \sigma_{i,M}^2)$. We propose a geometry-aligned noise allocation scheme for $\boldsymbol{\sigma}_i$ to achieve two privacy objectives. First, we aim at maximizing the numerical uncertainty of the estimated user location by the adversary, which is quantified by the expected mean squared error (MSE) between the estimated location $\tilde{\mathbf{p}}_{u,i}$ and the true location $\mathbf{p}_{u,i}$

$$P(\boldsymbol{\sigma}_i) \triangleq \mathbb{E}\{\|\tilde{\mathbf{p}}_{u,i} - \mathbf{p}_{u,i}\|_2^2\} \quad (34)$$

where $\tilde{\mathbf{p}}_{u,i}$ is the location estimate that is probably computed by the adversary. Based on our location leakage study in Table I for the adversary strategy (18), we simply pick the form

$$\tilde{\mathbf{p}}_{u,i} = \frac{\sum_{m=1}^M \tilde{G}_{i,m}^2 \mathbf{c}_m}{\sum_{m=1}^M \tilde{G}_{i,m}^2}. \quad (35)$$

Second, we also need to obfuscate the spatial pattern of the noise corrupted gradient $\tilde{G}_{i,m}$. An example is illustrated in Fig. 3, where in Fig. 3(b), if one only focused on the numerical confusion metric (34), the optimal choice will be allocating the entire noise budget to the grid cells on the edge. On the contrary, we hope to distribute noise smoothly over a large number of grid cells to cover the spatial pattern of the gradient as shown in Fig. 3(d).

Toward this end, we define a new metric, *spatial variance*, for the spatial smoothness of the noise corrupted gradient.

Definition 1 (Spatial Variance). The spatial variance across grid cells $m \in \{1, 2, \dots, M\}$ is defined as the expectation of the sample variance over this set of random variables $\{\tilde{G}_{i,m}^2\}$

$$V(\boldsymbol{\sigma}_i) \triangleq \mathbb{E}\left\{ \frac{1}{M} \sum_{m=1}^M \left(\tilde{G}_{i,m}^2 - \frac{1}{M} \sum_{n=1}^M \tilde{G}_{i,n}^2 \right)^2 \right\}. \quad (36)$$

It follows that if $\tilde{G}_{i,m}^2$ are spatially and statistically identical, the spatial variance is minimized as 0, achieving the best protection in terms of hiding the spatial pattern. Note that, this extreme spatial smoothness may require a large noise budget

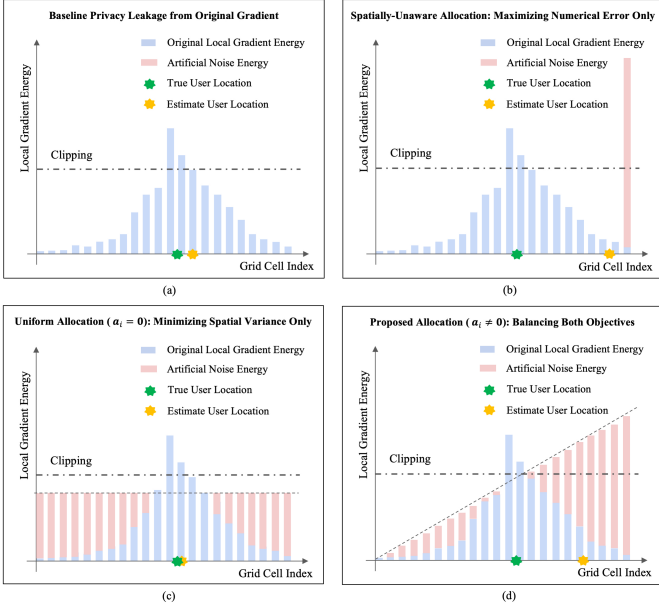


Figure 3. Illustration of the leaked location by the adversary strategy (18): (a) The original local gradient energy peaks near the true user location, leading to a significant privacy leakage under a WCL attack. (b) A spatially-unaware strategy that maximizes the localization error by placing all noise on the edge fails to obfuscate the gradient’s spatial pattern. (c) A uniform noise allocation ($\mathbf{a}_i = \mathbf{0}$) perfectly masks the spatial pattern but provides weak numerical protection against the adversary. (d) The proposed spatially-aware linear allocation ($\mathbf{a}_i \neq \mathbf{0}$) effectively balances both privacy objectives by simultaneously creating a large localization bias and masking the original gradient’s shape.

or a small gradient clipping parameter C , which significantly affects the convergence rate.

To ease the design and achieve a good trade-off between location privacy protection and convergence, we consider a spatially linear noise allocation pattern with slope \mathbf{a}_i and offset b_i . As a result, the square of the noise corrupted gradient $\tilde{G}_{i,m}^2$ roughly distributed above $\mathbf{a}_i^T \mathbf{c}_m + b_i$, where recall that \mathbf{c}_m is the coordinate of the m th grid cell.

Two numerical examples are given in Fig. 3, where the original clipped squared gradient $\tilde{G}_{i,m}^2$ are statistically centered near the user location (See Theorem 1). In Fig. 3(c), adding noise following slope $\mathbf{a}_i = \mathbf{0}$ can completely mask the spatial pattern of the gradient, achieving a spatial variance of 0 according to (36), but the location privacy protection is weak against adversary strategy (35). In Fig. 3(d), the noise is allocated such that the expected squared of the noise corrupted gradient $\tilde{G}_{i,m}^2$ are roughly masked by $\mathbf{a}_i^T \mathbf{c}_m + b_i$. Although the non-zero slope \mathbf{a}_i leads to a larger spatial variance under (36), it also contributes to location estimation bias under adversary strategy (35), achieving a better location privacy protection. Note that one can also clip the gradient to help bring down the spatial variance under the same total noise budget, at the cost of sacrificing the learning performance as indicated by Corollary 1.

Based on the above two design objectives, the noise budget for the m th grid cell is given as

$$\sigma_{i,m}^2 = \max\{0, \mathbf{a}_i^T \mathbf{c}_m + b_i - \tilde{G}_{i,m}^2\}. \quad (37)$$

The slope \mathbf{a}_i and the offset b_i are optimized to balance the numeric localization error (34) under the adversary strategy (35) and the spatial variance (36) that hides the spatial pattern of the gradient as

$$\underset{\mathbf{a}_i, b_i}{\text{maximize}} \quad P(\sigma_i) - \rho V(\sigma_i) \quad (38)$$

$$\text{subject to} \quad \sigma_{i,m}^2 = \max\{0, \mathbf{a}_i^T \mathbf{c}_m + b_i - \tilde{G}_{i,m}^2\} \quad (39)$$

$$\sum_{m=1}^M \sigma_{i,m}^2 \leq \mu \sum_{m=1}^M \tilde{G}_{i,m}^2. \quad (40)$$

where ρ is a non-negative hyper parameter that controls the trade-off between the two competing privacy objectives, and (40) controls the total noise budget.

Intuitively, the slope \mathbf{a}_i should be *aligned* with the localization bias of the adversary under the noise-free gradient \mathbf{g}_i . Consider the example illustrated in Fig. 3(a), where the location estimated by the adversary (35), or a more general WCL strategy, has a positive bias. If the slope \mathbf{a}_i is also positive, then the bias can be enlarged by adding noise to the gradient. Such a property is formally captured by theorem in the next subsection.

C. Algorithm for Adaptive Noise Allocation

The first term $P(\sigma_i)$ in the objective function (38) can be decomposed as follows.

Theorem 2 (Bias-Variance Decomposition). *As the number of grid cells $M \rightarrow \infty$ with a decreasing grid size, the squared localization error converges in probability to*

$$\|\tilde{\mathbf{p}}_{u,i} - \mathbf{p}_{u,i}\|_2^2 \rightarrow \frac{1}{(1 + \mu)^2} \|\Delta_g + \mu \Delta_n\|_2^2 \quad (41)$$

where the “bias” term is given as

$$\Delta_g = \frac{\sum_{m=1}^M \tilde{G}_{i,m}^2 \mathbf{c}_m}{\sum_{m=1}^M \tilde{G}_{i,m}^2} - \mathbf{p}_{u,i} \quad (42)$$

and the “variance” term due to the artificial noise is

$$\Delta_n = \frac{\sum_{m=1}^M \sigma_{i,m}^2 \mathbf{c}_m}{\sum_{m=1}^M \sigma_{i,m}^2} - \mathbf{p}_{u,i}. \quad (43)$$

Proof. See Appendix D. \square

Theorem 2 decomposes the total localization error into a weighted combination of two distinct vectors Δ_g and Δ_n . The key insight is that the magnitude of the resulting error vector $\Delta_g + \mu \Delta_n$ is asymptotically maximized when the “variance” vector Δ_n is *geometrically aligned* with the “bias” vector Δ_g . This principle provides an initial direction for the algorithm developed next to solve for the optimal plane parameters.

Theorem 2 provides an initialization strategy for an iterative algorithm that solves (38) under finite M . Specifically, the slope \mathbf{a}_i can be initialized as $\mathbf{a}_i = r_i \mathbf{u}_i$, where $\mathbf{u}_i = \Delta_g / \|\Delta_g\|_2$. The objective function (38) can be written as $J(\mathbf{u}_i, r_i, b_i) = P(\sigma_i(\mathbf{u}_i, r_i, b_i)) - \rho V(\sigma_i(\mathbf{u}_i, r_i, b_i))$. The algorithm can be developed using a nested structure, where in the outer loop, the unit direction vector \mathbf{u}_i is iteratively

updated using gradient descent. In the inner loop, for a fixed direction \mathbf{u}_i , the corresponding scalar coefficient r_i is optimized. Furthermore, for any given pair (\mathbf{u}_i, r_i) , the associated parameter b_i is uniquely determined and can be efficiently computed using a bisection search.

Algorithm 1 Geometry-Aligned Differential Privacy

Input: Clipped local gradient $\bar{\mathbf{g}}_i$; user location $\mathbf{p}_{u,i}$; privacy parameter μ ; trade-off control parameter ρ

Output: Differentially private gradient $\tilde{\mathbf{g}}_i$

- 1) Initialize the direction as $\mathbf{u}_i \leftarrow \frac{\Delta_{\mathbf{g}}}{\|\Delta_{\mathbf{g}}\|_2} \in \mathbb{R}^2$ and the step as $r_i \leftarrow r_{\max}$.
- 2) For the optimization of \mathbf{u}_i in outer loop do
 - a) For the optimization of r_i in inner loop do
 - i) Solve for b_i given unique (\mathbf{u}_i, r_i) in

$$\sum_{m=1}^M \max\{0, r_i \mathbf{u}_i^T \mathbf{c}_m + b_i - \bar{G}_{i,m}^2\} - \sum_{m=1}^M \mu \bar{G}_{i,m}^2 = 0 \quad (44)$$

via bisection method

- ii) Compute the numerical gradient for r_i as

$$\frac{\partial J}{\partial r_i} = \frac{1}{2\epsilon} (J(\mathbf{u}_i, r_i + \epsilon) - J(\mathbf{u}_i, r_i - \epsilon)) \quad (45)$$

- iii) Update r_i using gradient ascent
- b) End For until $\|\partial J / \partial r_i\|_2 \leq \tau_r$.
- c) Compute the numerical gradient for \mathbf{u}_i as

$$\nabla J = \begin{bmatrix} \frac{1}{2\epsilon} (J(\mathbf{u}_i + \epsilon \mathbf{e}_1, r_i) - J(\mathbf{u}_i - \epsilon \mathbf{e}_1, r_i)) \\ \frac{1}{2\epsilon} (J(\mathbf{u}_i + \epsilon \mathbf{e}_2, r_i) - J(\mathbf{u}_i - \epsilon \mathbf{e}_2, r_i)) \end{bmatrix} \quad (46)$$

where $\mathbf{e}_1 = [1, 0]^T$, $\mathbf{e}_2 = [0, 1]^T$ are two orthogonal unit vectors in the 2D plane.

- d) Update \mathbf{u}_i using the gradient ascent

- 3) End For until $\|\nabla J\|_2 \leq \tau_u$.
- 4) The optimal parameters (\mathbf{u}_i^*, r_i^*) are found, find b_i^* for (\mathbf{u}_i^*, r_i^*) via bisection search, and get the optimal noise allocation as

$$\sigma_{i,m}^{*2} = \max\{0, r_i^* \mathbf{u}_i^{*T} \mathbf{c}_m + b_i^* - \bar{G}_{i,m}^2\} \quad (47)$$

- 5) Noise Generation:

- a) Generate noise vector $\mathbf{n}_i \in \mathbb{R}^M$ where each component $n_{i,m} \sim \mathcal{N}(0, \sigma_{i,m}^{*2})$.
 - b) Construct the final noisy gradient: $\tilde{\mathbf{g}}_i \leftarrow \bar{\mathbf{g}}_i + \mathbf{n}_i$.
-

The proposed geometry-aligned differential privacy algorithm is guaranteed to converge to a stationary, locally optimal solution. At each iteration, the algorithm uses a one-dimensional bisection search to solve a monotonic root-finding problem for b_i , ensuring a unique solution for this parameter. Building on this, gradient ascent updates for r_i and \mathbf{u}_i , within a compact search space, monotonically increase the continuous objective function $J(\mathbf{u}_i, r_i, b_i)$. Since J is bounded above due to finite localization error and spatial variance, the resulting non-decreasing sequence of objective values will converge. Therefore, the algorithm converges to a stationary point $(\mathbf{u}_i^*, r_i^*, b_i^*)$ that satisfies the first-order optimality conditions of the privacy maximization problem.

Table II
RADIO MAP RECONSTRUCTION MAE (dB) VS. TRAINING EPOCH FOR DIFFERENT PRIVACY BUDGETS μ

	μ	Epoch 1	Epoch 50	Epoch 100	Epoch 200
Proposed	1	13.68	6.72	4.01	3.92
	10	13.68	6.79	4.11	4.05
	50	13.68	6.85	4.21	4.25
FedAvg		13.68	6.68	3.98	3.81

V. NUMERICAL RESULTS

In this section, we present simulation results to validate the performance of our proposed geometry-aligned differential privacy algorithm on radio map federated construction. The simulations are conducted in a detailed 300 m \times 300 m dense urban environment, populated with buildings of diverse geometries, including circular, cubic, and irregular shapes, and heights ranging from 10 m to 130 m. This virtual city comprises 100 randomly distributed ground users and 200 aerial base stations operating at a 50 m altitude. Each user collects 200 channel measurements from these base stations, and the entire area is discretized into a grid of 3 m \times 3 m cells for the purpose of model reconstruction. The subsequent sections will analyze the radio map accuracy and the effectiveness of our privacy-preserving mechanism within this setting.

A. Radio Map Construction Performance

In this section, we evaluate the impact of the privacy-preserving noise, governed by the parameter μ on the radio map reconstruction accuracy. We compare its performance with the standard Federated Averaging (FedAvg) algorithm, which serves as a baseline and represents the ideal performance without noise. In the evaluation, the noise allocation parameter is fixed at $\rho = 50$ and the clipping threshold is set to $C = 1$. We train the geometry-aligned differential privacy algorithm under a range of distinct privacy budgets, by varying μ across the set $\{0.5, 1, 5, 10, 20, 50\}$. The reconstruction performance is quantified by the MAE of the predicted channel gain over the entire geographical area. The convergence behavior for different μ values is illustrated by the MAE during each training iteration, with detailed results presented in Table II. Table II shows that the non-private FedAvg baseline achieves a final MAE of 3.81 dB, while our geometry-aligned DP method reaches 4.25 dB at $\mu = 50$. This 0.44 dB increase is marginal, demonstrating a highly favorable privacy-utility trade-off.

B. Location Privacy Protection Performance

This section evaluates the privacy protection afforded by our proposed geometry-aligned differential privacy algorithm against the WCL adversary described in Section 3.2. The performance is measured by the estimated localization error by adversary—the distance between a user's true location and the one inferred by the WCL attack. A greater error corresponds to a higher degree of privacy. We analyze the influence of two key

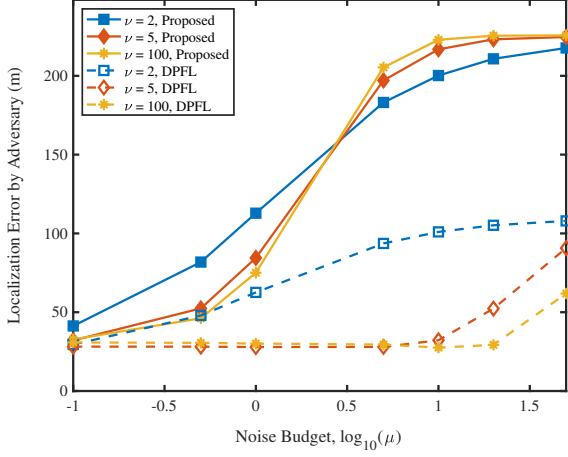


Figure 4. Localization error by adversary vs. noise budget μ for different parameter ν used by the adversary. The proposed scheme achieves substantially better protection over all parameters.

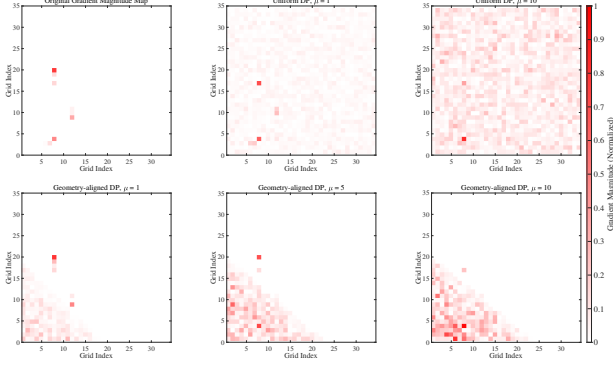


Figure 5. Gradient magnitude maps under increasing noise budgets for the uniform DP baseline (top row) and the geometry-aligned DP scheme (bottom row). As μ increases, the geometry-aligned DP obfuscates spatial gradient patterns while controlling the adversary's localization error, illustrating the trade-off between pattern concealment and the numerical location-privacy metric.

parameters: the total noise budget μ and the geometric trade-off parameter ρ , which controls the spatial allocation of noise. Throughout the evaluation, the clipping threshold is fixed at $C = 1$.

1) *Impact of Noise Budget μ on Privacy:* We evaluate the impact of the noise budget μ by comparing our geometry-aligned differential privacy algorithm with a uniform-noise Differential Privacy Federated Learning (DPFL) baseline. In this analysis, the geometric trade-off parameter of the proposed algorithm is fixed to $\rho = 1$. As shown in Fig. 4, increasing the noise budget μ raises the adversary's localization error for both the geometry-aligned DP scheme and the uniform DPFL baseline. For any given μ , the error induced by our strategy is substantially larger than that from DPFL across all tested attacker power values ν .

This robust privacy gain stems from injecting structured noise that shifts the gradient's perceived centroid rather than simply diffusing it. In contrast to uniform noise, which merely obscures the original gradient, the geometry-aligned noise

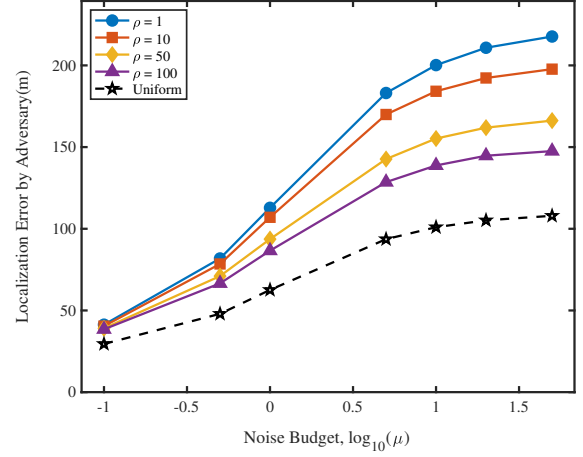


Figure 6. Estimated adversarial localization error vs. geometric trade-off parameter ρ (with adversary power $\nu = 2$). Smaller ρ values produce the higher localization errors, whereas larger ρ slightly reduces the error; all proposed noise allocations still outperform the uniform noise baseline in terms of adversary error.

produces a deliberate spatial pattern that becomes more pronounced with larger μ as shown in Fig. 5. This pattern actively misleads the WCL adversary and amplifies the localization error.

2) *Efficacy of Adaptive Noise Allocation ρ :* Fig. 6 shows that smaller values of the trade-off parameter ρ produce higher adversarial localization errors. With $\rho = 1$, the noise is concentrated in a high-impact region, yielding the maximum adversary error exceeding 220 m at large μ . Increasing ρ spreads the noise more evenly, which slightly reduces the peak error to approximately 150m at $\rho = 100$ but results in a more diffuse gradient perturbation. This effect is evident in the gradient maps: a small ρ creates a localized noise pattern, whereas a large ρ distributes noise broadly. Importantly, every geometry-aligned configuration still induces much higher adversary error than the uniform baseline.

VI. CONCLUSION

This paper investigated the vulnerability of federated radio map construction to location inference attacks. Spatially decaying gradient patterns were identified as a key source of location information leakage. To counter this threat, we proposed a geometry-aligned differential privacy framework. This method injects heterogeneous noise into the model updates to obscure spatial gradient patterns and degrade the localization performance of adversary strategies, thus enhancing the location privacy of the users. A theoretical convergence bound was derived to quantify the trade-off between privacy and utility for the proposed approach. It is shown that the federated training algorithm converges to a stationary point with a bounded expected gradient norm under the proposed non-uniform noise scheme. Simulations showed that the framework can improve location privacy by raising the adversary's localization error from 30m to over 180m. This privacy gain was achieved with

only a 0.2dB degradation in map accuracy compared to a uniform noise baseline.

APPENDIX A PROOF OF THEOREM 1

Denote the component of the local gradient element as

$$g_{i,j,m} = \Gamma(\mathbf{p}_j; \mathbf{h}) D(\mathbf{p}_j; \mathbf{h}, m). \quad (48)$$

Thus, the local gradient element (16) simplifies to

$$G_{i,m} = \frac{2}{J_i} \sum_{j \in \mathcal{N}_{i,m}} g_{i,j,m}. \quad (49)$$

To facilitate the monotonicity discussion of $G_{i,m}$, we first investigate the sign property of the component $g_{i,j,m}$. Based on (13), according that the actual channel gain is formulated as $y_j = \gamma(\mathbf{p}_j; \mathbf{h}^*) + \xi_j$, the product term $\Gamma(\mathbf{p}_j; \mathbf{h})$ in the component $g_{i,j,m}$ is split into

$$\Gamma(\mathbf{p}_j; \mathbf{h}) = \hat{\Gamma}(\mathbf{p}_j; \mathbf{h}) + \hat{\xi}_j \quad (50)$$

where

$$\begin{aligned} \hat{\Gamma}(\mathbf{p}_j; \mathbf{h}) &= (\gamma(\mathbf{p}_j; \mathbf{h}^*) - \gamma(\mathbf{p}_j; \mathbf{h})) \\ &\quad \times ((\beta_1 + \alpha_1 \log_{10} d(\mathbf{p}_j)) \\ &\quad - (\beta_0 + \alpha_0 \log_{10} d(\mathbf{p}_j))) \\ &= ((\beta_1 + \alpha_1 \log_{10} d(\mathbf{p}_j)) - (\beta_0 + \alpha_0 \log_{10} d(\mathbf{p}_j)))^2 \\ &\quad \times (S(\mathbf{p}_j; \mathbf{h}^*) - S(\mathbf{p}_j; \mathbf{h})) \end{aligned} \quad (51)$$

is the model error term whose sign depends on the model difference $(S(\mathbf{p}_j; \mathbf{h}^*) - S(\mathbf{p}_j; \mathbf{h}))$, and

$$\hat{\xi}_j = \xi_j((\beta_1 + \alpha_1 \log_{10} d(\mathbf{p}_j)) - (\beta_0 + \alpha_0 \log_{10} d(\mathbf{p}_j))) \quad (52)$$

is the noise term, a product of Gaussian noise and a constant, still Gaussian noise. Thus, based on (48), (50), the component of the local gradient element $g_{i,j,m}$ is split into the real model value and the noise as

$$\begin{aligned} g_{i,j,m} &= \tilde{g}_{i,j,m} + \tilde{\xi}_{i,j,m} \\ &= \hat{\Gamma}(\mathbf{p}_j; \mathbf{h}) D(\mathbf{p}_j; \mathbf{h}, m) + \hat{\xi}_j D(\mathbf{p}_j; \mathbf{h}, m) \end{aligned} \quad (53)$$

where the noise term $\tilde{\xi}_{i,j,m}$ is the product of Gaussian noise and a constant, still Gaussian noise. According to (14), the term $D(\mathbf{p}_j; \mathbf{h}, m)$ is always positive.

Therefore, for the expansion of the model error term $\tilde{g}_{i,j,m}, \forall j \in \mathcal{N}_{i,m}$ in (53), the product terms except for $(S(\mathbf{p}_j; \mathbf{h}^*) - S(\mathbf{p}_j; \mathbf{h}))$ are always positive. To explore the sign of $g_{i,j,m}$, we only focus on the sign of the difference term $(S(\mathbf{p}_j; \mathbf{h}^*) - S(\mathbf{p}_j; \mathbf{h}))$. According to (14), (3), when $\mathbf{h}^* \prec \mathbf{h}$, the expectations of the contributing gradient components $\tilde{g}_{i,j,m}, \forall j \in \mathcal{N}_{i,m}$ are consistently greater than 0. On the contrary, when $\mathbf{h}^* \succ \mathbf{h}$, the expectations of the contributing gradient components $\tilde{g}_{i,j,m}, \forall j \in \mathcal{N}_{i,m}$ are consistently less than 0.

Next we analyze the property of the sum $G_{i,m}$. According to the expansion (49), the expectation of the m th local gradient element is formulated as

$$\mathbb{E}\{G_{i,m}^2\} = \left(\frac{2}{J_i}\right)^2 \mathbb{E}\left\{\left(\sum_{j \in \mathcal{N}_{i,m}} g_{i,j,m}\right)^2\right\}. \quad (54)$$

Combined with (53), it is further computed as

$$\mathbb{E}\{G_{i,m}^2\} = \left(\frac{2}{J_i}\right)^2 \mathbb{E}\left\{\left(\sum_{j \in \mathcal{N}_{i,m}} (\tilde{g}_{i,j,m} + \tilde{\xi}_{i,j,m})\right)^2\right\}.$$

Thus, the expectation of the local gradient element $\mathbb{E}\{G_{i,m}^2\}$ is extended into

$$\begin{aligned} \mathbb{E}\{G_{i,m}^2\} &= \left(\frac{2}{J_i}\right)^2 \left(\mathbb{E}\left\{\sum_{j \in \mathcal{N}_{i,m}} \tilde{g}_{i,j,m}^2\right\} \right. \\ &\quad + \mathbb{E}\left\{\sum_{j \in \mathcal{N}_{i,m}} \tilde{\xi}_{i,j,m}^2\right\} \\ &\quad \left. + \mathbb{E}\left\{\sum_{\substack{j, j' \in \mathcal{N}_{i,m} \\ j \neq j'}} \tilde{g}_{i,j,m} \tilde{g}_{i,j',m}\right\} \right). \end{aligned}$$

The expectation of the $(m-1)$ th element of the local gradient is computed as

$$\begin{aligned} \mathbb{E}\{G_{i,m-1}^2\} &= \left(\frac{2}{J_i}\right)^2 \left(\mathbb{E}\left\{\sum_{j \in \mathcal{N}_{i,m-1}} \hat{g}_{i,j,m-1}^2\right\} \right. \\ &\quad + \mathbb{E}\left\{\sum_{j \in \mathcal{N}_{i,m-1}} \hat{\xi}_j^2\right\} \\ &\quad \left. + \mathbb{E}\left\{\sum_{\substack{j, j' \in \mathcal{N}_{i,m-1} \\ j \neq j'}} \hat{g}_{i,j,m-1} \hat{g}_{i,j',m-1}\right\} \right). \end{aligned}$$

As established previously, all $\tilde{g}_{i,j,m}$ for $j \in \mathcal{N}_{i,m}$ share the same sign. Consequently, this cross-product term is non-negative. We now compare the terms in the expansions of $\mathbb{E}\{G_{i,m}^2\}$ and $\mathbb{E}\{G_{i,m-1}^2\}$. The geometric property of spatial coverage implies a nesting relationship for the sets of influential measurements

$$\mathcal{N}_{i,m} \subseteq \mathcal{N}_{i,m-1}. \quad (55)$$

Since all three components in the expansion of $\mathbb{E}\{G_{i,m}^2\}$ are composed of non-negative summation terms, the reduction in the size of the summation set from $\mathcal{N}_{i,m-1}$ to $\mathcal{N}_{i,m}$ directly implies:

$$\mathbb{E}\{G_{i,m}^2\} \leq \mathbb{E}\{G_{i,m-1}^2\}. \quad (56)$$

This completes the proof.

APPENDIX B PROOF OF LEMMA 1

We first derive the expectation of the decrease in the loss function with respect to $\mathbf{h}(t)$ given $\boldsymbol{\theta}(t)$ in each round of training. First, by using the L -smoothness property in (23), we have

$$\begin{aligned} \mathbb{E}\{F(\mathbf{h}(t+1), \boldsymbol{\theta}(t))\} \\ \leq \mathbb{E}\{F(\mathbf{h}(t), \boldsymbol{\theta}(t))\} - \mathbb{E}\{\langle \mathbf{g}(t), \mathbf{h}(t+1) - \mathbf{h}(t) \rangle\} \\ + \frac{L}{2} \mathbb{E}\{\|\mathbf{h}(t+1) - \mathbf{h}(t)\|_2^2\}. \end{aligned} \quad (57)$$

Recall that the update local gradient is $\tilde{\mathbf{g}}_i(t) = \bar{\mathbf{g}}_i(t) + \mathbf{n}_i(t)$. Under the DP policy, the aggregation for $\mathbf{h}(t+1)$ in (10) becomes

$$\begin{aligned}\mathbf{h}(t+1) &= \mathbf{h}(t) + \eta_h \sum_{i=1}^N \frac{J_i}{J} \tilde{\mathbf{g}}_i(t) \\ &= \mathbf{h}(t) + \eta_h \sum_{i=1}^N \frac{J_i}{J} \bar{\mathbf{g}}_i(t) + \eta_h \sum_{i=1}^N \frac{J_i}{J} \mathbf{n}_i(t).\end{aligned}\quad (58)$$

In this case, (57) is derived as

$$\begin{aligned}\mathbb{E}\{F(\mathbf{h}(t+1), \boldsymbol{\theta}(t))\} \\ \leq \mathbb{E}\{F(\mathbf{h}(t), \boldsymbol{\theta}(t))\} \\ - \eta_h \mathbb{E}\{\langle \mathbf{g}(t), \sum_{i=1}^N \frac{J_i}{J} \bar{\mathbf{g}}_i(t) + \eta_h \sum_{i=1}^N \frac{J_i}{J} \mathbf{n}_i(t) \rangle\} \\ + \frac{L\eta_h^2}{2} \mathbb{E}\{\|\sum_{i=1}^N \frac{J_i}{J} \bar{\mathbf{g}}_i(t) + \sum_{i=1}^N \frac{J_i}{J} \mathbf{n}_i(t)\|_2^2\}.\end{aligned}\quad (59)$$

Since the expectation of the noise $\mathbb{E}\{\mathbf{n}_i(t)\} = 0$ and the noise is independent of the gradients, (59) is simplified as

$$\begin{aligned}\mathbb{E}\{F(\mathbf{h}(t+1), \boldsymbol{\theta}(t))\} \\ \leq \mathbb{E}\{F(\mathbf{h}(t), \boldsymbol{\theta}(t))\} - \eta_h \mathbb{E}\{\langle \mathbf{g}(t), \sum_{i=1}^N \frac{J_i}{J} \bar{\mathbf{g}}_i(t) \rangle\} \\ + \frac{L\eta_h^2}{2} (\mathbb{E}\{\|\sum_{i=1}^N \frac{J_i}{J} \bar{\mathbf{g}}_i(t)\|_2^2\} + \mathbb{E}\{\|\sum_{i=1}^N \frac{J_i}{J} \mathbf{n}_i(t)\|_2^2\}).\end{aligned}\quad (60)$$

Now, we first simplify the last line of (60). For the first term $\mathbb{E}\{\|\sum_{i=1}^N \frac{J_i}{J} \bar{\mathbf{g}}_i(t)\|_2^2\}$, we use Jensen's inequality and the fact that clipping only reduces the norm, i.e., $\|\bar{\mathbf{g}}_i(t)\|_2 \leq \|\mathbf{g}_i(t)\|_2$, and derive that

$$\begin{aligned}\mathbb{E}\{\|\sum_{i=1}^N \frac{J_i}{J} \bar{\mathbf{g}}_i(t)\|_2^2\} &\leq \mathbb{E}\{\|\sum_{i=1}^N \frac{J_i}{J} \mathbf{g}_i(t)\|_2^2\} \\ &\leq \sum_{i=1}^N \frac{J_i}{J} \mathbb{E}\{\|\mathbf{g}_i(t)\|_2^2\}.\end{aligned}\quad (61)$$

For the second term, using the independence of noise across users and Assumption 2

$$\begin{aligned}\mathbb{E}\{\|\sum_{i=1}^N \frac{J_i}{J} \mathbf{n}_i(t)\|_2^2\} &= \sum_{i=1}^N \frac{J_i^2}{J^2} \mathbb{E}\{\|\mathbf{n}_i(t)\|_2^2\} \\ &\leq \sum_{i=1}^N \frac{J_i^2}{J^2} \mu \mathbb{E}\{\|\bar{\mathbf{g}}_i(t)\|_2^2\}.\end{aligned}\quad (62)$$

Combining (61) and (62) back into (60), we have

$$\begin{aligned}\mathbb{E}\{F(\mathbf{h}(t+1), \boldsymbol{\theta}(t))\} \\ \leq \mathbb{E}\{F(\mathbf{h}(t), \boldsymbol{\theta}(t))\} - \eta_h \mathbb{E}\{\langle \mathbf{g}(t), \sum_{i=1}^N \frac{J_i}{J} \bar{\mathbf{g}}_i(t) \rangle\} \\ + \frac{L\eta_h^2}{2} \sum_{i=1}^N (\frac{J_i}{J} + \mu \frac{J_i^2}{J^2}) \mathbb{E}\{\|\mathbf{g}_i(t)\|_2^2\}.\end{aligned}\quad (63)$$

Now, applying Assumption 1, we have

$$\begin{aligned}\mathbb{E}\{F(\mathbf{h}(t+1), \boldsymbol{\theta}(t))\} \\ \leq \mathbb{E}\{F(\mathbf{h}(t), \boldsymbol{\theta}(t))\} - \eta_h \mathbb{E}\{\langle \mathbf{g}(t), \sum_{i=1}^N \frac{J_i}{J} \bar{\mathbf{g}}_i(t) \rangle\} \\ + \frac{L\eta_h^2 B^2}{2} (1 + \mu \tilde{J}) \mathbb{E}\{\|\mathbf{g}(t)\|_2^2\}.\end{aligned}\quad (64)$$

where we use $\sum \frac{J_i}{J} = 1$ and $\tilde{J} = \sum \frac{J_i^2}{J^2}$.

We next simplify the cross-term in the second line of (64) as

$$\mathbb{E}\langle \mathbf{g}(t), \sum_{i=1}^N \frac{J_i}{J} \bar{\mathbf{g}}_i(t) \rangle = \mathbb{E}\langle \mathbf{g}(t), \bar{\mathbf{g}}(t) \rangle \quad (65)$$

where $\bar{\mathbf{g}}(t) = \sum_{i=1}^N \frac{J_i}{J} \bar{\mathbf{g}}_i(t)$ denotes the aggregation of the clipped gradient.

To investigate the bias introduced by gradient clipping, we define $\mathbf{b}_i(t) = \mathbf{g}_i(t) - \bar{\mathbf{g}}_i(t)$ be the clipped-off portion for user i . Then, the global bias $\mathbf{b}(t) = \sum_{i=1}^N \frac{J_i}{J} \mathbf{b}_i(t)$. If $\|\mathbf{g}_i(t)\|_2 \leq C$, then $\mathbf{b}_i(t) = \mathbf{0}$. If $\|\mathbf{g}_i(t)\|_2 > C$, then $\mathbf{b}_i(t) = \mathbf{g}_i(t) \left(1 - \frac{C}{\|\mathbf{g}_i(t)\|_2}\right)$. The norm is $\|\mathbf{b}_i(t)\|_2 = \|\mathbf{g}_i(t)\|_2 - C$, which is bounded as

$$\|\mathbf{b}_i(t)\|_2 = \frac{\|\mathbf{g}_i(t)\|_2^2 - C^2}{\|\mathbf{g}_i(t)\|_2 + C} < \frac{\|\mathbf{g}_i(t)\|_2^2}{2C}. \quad (66)$$

This bound holds trivially when $\|\mathbf{g}_i(t)\|_2 \leq C$ as well. Using Jensen's inequality for the aggregated bias, the expectation of the global bias norm is derived as

$$\begin{aligned}\mathbb{E}\{\|\mathbf{b}(t)\|_2^2\} &= \mathbb{E}\{\|\sum_{i=1}^N \frac{J_i}{J} \mathbf{b}_i(t)\|_2^2\} \leq \mathbb{E}\{\sum_{i=1}^N \frac{J_i}{J} \|\mathbf{b}_i(t)\|_2^2\} \\ &< \mathbb{E}\{\sum_{i=1}^N \frac{J_i}{J} (\frac{\|\mathbf{g}_i(t)\|_2^2}{2C})^2\} = \frac{1}{4C^2} \mathbb{E}\{\|\mathbf{g}_i(t)\|_2^4\} \\ &\leq \frac{B^4 L^4}{4C^2}.\end{aligned}\quad (67)$$

Thus, the cross-term in the second line $\mathbb{E}\langle \mathbf{g}(t), \bar{\mathbf{g}}(t) \rangle$ is derived as

$$\begin{aligned}\mathbb{E}\{\langle \mathbf{g}(t), \bar{\mathbf{g}}(t) \rangle\} &= \mathbb{E}\{\langle \mathbf{g}(t), \mathbf{g}(t) - \mathbf{b}(t) \rangle\} \\ &\geq \mathbb{E}\{\|\mathbf{g}(t)\|_2^2\} \\ &\quad - \frac{1}{2} (\mathbb{E}\{\|\mathbf{g}(t)\|_2^2\} + \mathbb{E}\{\|\mathbf{b}(t)\|_2^2\}) \\ &= \frac{1}{2} \mathbb{E}\{\|\mathbf{g}(t)\|_2^2\} - \frac{1}{2} \mathbb{E}\{\|\mathbf{b}(t)\|_2^2\}.\end{aligned}\quad (68)$$

Substituting (68) into (64), we get

$$\begin{aligned}\mathbb{E}\{F(\mathbf{h}(t+1), \boldsymbol{\theta}(t))\} - \mathbb{E}\{F(\mathbf{h}(t), \boldsymbol{\theta}(t))\} \\ \leq -\eta_h (\frac{1}{2} \mathbb{E}\{\|\mathbf{g}(t)\|_2^2\} - \frac{1}{2} \mathbb{E}\{\|\mathbf{b}(t)\|_2^2\}) \\ + \frac{L\eta_h^2 B^2}{2} (1 + \mu \tilde{J}) \mathbb{E}\{\|\mathbf{g}(t)\|_2^2\} \\ = -\eta_h (\frac{1}{2} - \frac{L\eta_h B^2}{2} (1 + \mu \tilde{J})) \mathbb{E}\{\|\mathbf{g}(t)\|_2^2\} + \frac{\eta_h B^4 L^4}{8C^2}.\end{aligned}\quad (69)$$

The proof of the first conclusion in Lemma 1 is completed.

Then, we analyze the update of θ from $(\mathbf{h}(t+1), \theta(t))$ to $(\mathbf{h}(t+1), \theta(t+1))$. Using L -smoothness with respect to θ , we have

$$\begin{aligned} F(\mathbf{h}(t+1), \theta(t+1)) &\leq F(\mathbf{h}(t+1), \theta(t)) \\ &\quad + \nabla F(\theta(t); \mathbf{h}(t+1))^\top \\ &\quad \times (\theta(t+1) - \theta(t)) \\ &\quad + \frac{L}{2} \|\theta(t+1) - \theta(t)\|^2. \end{aligned} \quad (70)$$

Recall the standard update rule for propagation parameter θ in (11), we get

$$\theta(t+1) - \theta(t) = -\eta_\theta \nabla F(\theta(t); \mathbf{h}(t+1)). \quad (71)$$

Substituting (71) into (70), we have

$$\begin{aligned} F(\mathbf{h}(t+1), \theta(t+1)) &\leq F(\mathbf{h}(t+1), \theta(t)) \\ &\quad - \eta_\theta \|\nabla F(\theta(t); \mathbf{h}(t+1))\|^2 \\ &\quad + \frac{L\eta_\theta^2}{2} \|\nabla F(\theta(t); \mathbf{h}(t+1))\|^2. \end{aligned} \quad (72)$$

We take the expectation of the randomness introduced by the update of \mathbf{h} , and get

$$\begin{aligned} \mathbb{E}\{F(\mathbf{h}(t+1), \theta(t+1)) - F(\mathbf{h}(t+1), \theta(t))\} \\ \leq -\kappa_\theta \mathbb{E}\{\|\nabla F(\theta(t); \mathbf{h}(t+1))\|^2\} \end{aligned} \quad (73)$$

where $\kappa_\theta = \eta_\theta - \frac{L\eta_\theta^2}{2}$.

APPENDIX C PROOF OF COROLLARY 1

Recall the initial bound (30)

$$\begin{aligned} \frac{1}{T} \sum_{t=0}^{T-1} \mathbb{E}\{\|\nabla F(\mathbf{h}(t), \theta(t))\|_2^2\} \\ \leq \frac{\mathbb{E}\{F(\mathbf{h}(0), \theta(0)) - F(\mathbf{h}(T), \theta(T))\}}{T\kappa} + \frac{\eta_h B^4 L^4}{8C^2 \kappa}. \end{aligned} \quad (74)$$

Since the difference of the function $F(\mathbf{h}, \theta)$ is bounded, when $T \rightarrow \infty$, the first on the right hand side tends to 0. It is derived that

$$\frac{1}{T} \sum_{t=0}^{T-1} \mathbb{E}\{\|\nabla F(\mathbf{h}(t), \theta(t))\|_2^2\} \leq \frac{\eta_h B^4 L^4}{8C^2 \kappa} \quad (75)$$

Thus after a sufficient number of iterations, this bound is reduced to

$$\mathbb{E}\{\|\nabla F(\mathbf{h}(t), \theta(t))\|_2^2\} \leq \frac{\eta_h B^4 L^4}{8C^2 \kappa}. \quad (76)$$

Applying the Jensen's inequality, we have

$$\mathbb{E}\{\|\nabla F(\mathbf{h}(t), \theta(t))\|_2^2\} \leq \mathbb{E}\{\|\nabla F(\mathbf{h}(t), \theta(t))\|_2\}^2. \quad (77)$$

Combining (76) and (77), we derive

$$\mathbb{E}\{\|\nabla F(\mathbf{h}(t), \theta(t))\|\} \leq \sqrt{\frac{\eta_h B^4 L^4}{8C^2 \kappa}}. \quad (78)$$

The proof is completed.

APPENDIX D PROOF OF THEOREM 2

We explore the approximation of the localization error by adversary under noisy gradient in a probabilistic sense as $M \rightarrow \infty$

$$\begin{aligned} \tilde{\mathbf{p}}_{u,i} - \mathbf{p}_{u,i} &\triangleq \frac{\sum_{m=1}^M \tilde{G}_{i,m}^2 \mathbf{c}_m}{\sum_{m=1}^M \tilde{G}_{i,m}^2} - \mathbf{p}_{u,i} \\ &= \frac{\sum_{m=1}^M \tilde{G}_{i,m}^2 (\mathbf{c}_m - \mathbf{p}_{u,i})}{\sum_{m=1}^M \tilde{G}_{i,m}^2}. \end{aligned} \quad (79)$$

Recall that the noisy gradient is defined as

$$\tilde{G}_{i,m} = \bar{G}_{i,m} + n_{i,m} \quad (80)$$

where $n_{i,m} \sim \mathcal{N}(0, \sigma_{i,m}^2)$ is independent Gaussian noise. Substituting (80) into (79), the localization error by adversary is then expanded to

$$\begin{aligned} \tilde{\mathbf{p}}_{u,i} - \mathbf{p}_{u,i} &= \frac{\sum_{m=1}^M (\bar{G}_{i,m} + n_{i,m})^2 (\mathbf{c}_m - \mathbf{p}_{u,i})}{\sum_{m=1}^M (\bar{G}_{i,m} + n_{i,m})^2} \\ &= \frac{\sum_{m=1}^M (\bar{G}_{i,m}^2 + 2\bar{G}_{i,m}n_{i,m} + n_{i,m}^2) (\mathbf{c}_m - \mathbf{p}_{u,i})}{\sum_{m=1}^M (\bar{G}_{i,m}^2 + 2\bar{G}_{i,m}n_{i,m} + n_{i,m}^2)}. \end{aligned} \quad (81)$$

Here the squared noise term is decomposed as

$$\sum_{m=1}^M n_{i,m}^2 = \sum_{m=1}^M \sigma_{i,m}^2 + \sum_{m=1}^M (n_{i,m}^2 - \sigma_{i,m}^2). \quad (82)$$

Thus, the complete expansion of the localization error is derived as (83). In (83), $\sum_{m=1}^M (n_{i,m}^2 - \sigma_{i,m}^2)$ is the random fluctuation term with zero mean and variance

$$\text{Var} \left(\sum_{m=1}^M (n_{i,m}^2 - \sigma_{i,m}^2) \right) = \sum_{m=1}^M \text{Var}(n_{i,m}^2) = \sum_{m=1}^M 2\sigma_{i,m}^4. \quad (84)$$

Similarly, the cross term $2 \sum_{m=1}^M \bar{G}_{i,m} n_{i,m}$ has zero mean and variance:

$$\text{Var} \left(2 \sum_{m=1}^M \bar{G}_{i,m} n_{i,m} \right) = 4 \sum_{m=1}^M \bar{G}_{i,m}^2 \sigma_{i,m}^2. \quad (85)$$

Considering that the grid cells $\{\mathbf{c}_m\}$ are uniform in a bounded region, with fixed total gradient power $\sum_{m=1}^M \bar{G}_{i,m}^2 \sim O(1)$ and noise budget $\sum_{m=1}^M \sigma_{i,m}^2 = \mu \sum_{m=1}^M \bar{G}_{i,m}^2 \sim O(1)$, the typical magnitudes are $\bar{G}_{i,m}, \sigma_{i,m} \sim O(1/\sqrt{M})$. Consequently, the variance of the cross term is

$$4 \sum_{m=1}^M \bar{G}_{i,m}^2 \sigma_{i,m}^2 \sim O \left(4M \cdot \frac{1}{M^2} \right) = O \left(\frac{1}{M} \right). \quad (86)$$

The variance of the quadratic fluctuation term is

$$\sum_{m=1}^M 2\sigma_{i,m}^4 \sim O \left(2M \cdot \frac{1}{M^2} \right) = O \left(\frac{1}{M} \right). \quad (87)$$

By the Chebyshev's inequality, as $M \rightarrow \infty$, these fluctuation terms $\sum_{m=1}^M (n_{i,m}^2 - \sigma_{i,m}^2)$ and $2 \sum_{m=1}^M \bar{G}_{i,m} n_{i,m}$

$$\tilde{\mathbf{p}}_{u,i} - \mathbf{p}_{u,i} = \frac{\sum_{m=1}^M (\bar{G}_{i,m}^2 + \sigma_{i,m}^2)(\mathbf{c}_m - \mathbf{p}_{u,i}) + 2 \sum_{m=1}^M \bar{G}_{i,m} n_{i,m}(\mathbf{c}_m - \mathbf{p}_{u,i}) + \sum_{m=1}^M (n_{i,m}^2 - \sigma_{i,m}^2)(\mathbf{c}_m - \mathbf{p}_{u,i})}{\sum_{m=1}^M (\bar{G}_{i,m}^2 + \sigma_{i,m}^2) + 2 \sum_{m=1}^M \bar{G}_{i,m} n_{i,m} + \sum_{m=1}^M (n_{i,m}^2 - \sigma_{i,m}^2)} \quad (83)$$

vanish in probability. Thus, the attacker localization error is approximated as

$$\tilde{\mathbf{p}}_{u,i} - \mathbf{p}_{u,i} \approx \frac{\sum_{m=1}^M (\bar{G}_{i,m}^2 + \sigma_{i,m}^2)(\mathbf{c}_m - \mathbf{p}_{u,i})}{\sum_{m=1}^M (\bar{G}_{i,m}^2 + \sigma_{i,m}^2)} \quad (88)$$

It is divided into two components as

$$\begin{aligned} \tilde{\mathbf{p}}_{u,i} - \mathbf{p}_{u,i} &\approx \frac{\sum_{m=1}^M \bar{G}_{i,m}^2 (\mathbf{c}_m - \mathbf{p}_{u,i})}{\sum_{m=1}^M (\bar{G}_{i,m}^2 + \sigma_{i,m}^2)} + \frac{\sum_{m=1}^M \sigma_{i,m}^2 (\mathbf{c}_m - \mathbf{p}_{u,i})}{\sum_{m=1}^M (\bar{G}_{i,m}^2 + \sigma_{i,m}^2)} \end{aligned} \quad (89)$$

With the maximum noise budget $\sum_{m=1}^M \sigma_{i,m}^2 \leq \mu \sum_{m=1}^M \bar{G}_{i,m}^2$ in (22), it is further reduced to

$$\begin{aligned} \tilde{\mathbf{p}}_{u,i} - \mathbf{p}_{u,i} &\approx \frac{\sum_{m=1}^M \bar{G}_{i,m}^2 (\mathbf{c}_m - \mathbf{p}_{u,i})}{(1 + \mu) \sum_{m=1}^M \bar{G}_{i,m}^2} + \frac{\sum_{m=1}^M \sigma_{i,m}^2 (\mathbf{c}_m - \mathbf{p}_{u,i})}{(1 + \mu) \sum_{m=1}^M \bar{G}_{i,m}^2} \\ &= \frac{\sum_{m=1}^M \bar{G}_{i,m}^2 (\mathbf{c}_m - \mathbf{p}_{u,i})}{(1 + \mu) \sum_{m=1}^M \bar{G}_{i,m}^2} + \frac{\mu \sum_{m=1}^M \sigma_{i,m}^2 (\mathbf{c}_m - \mathbf{p}_{u,i})}{(1 + \mu) \sum_{m=1}^M \bar{G}_{i,m}^2} \end{aligned} \quad (90)$$

where

$$\Delta_g \triangleq \frac{\sum_{m=1}^M \bar{G}_{i,m}^2 \mathbf{c}_m}{\sum_{m=1}^M \bar{G}_{i,m}^2} - \mathbf{p}_{u,i} \quad (91)$$

is the error component introduced by gradient clipping, and

$$\Delta_n \triangleq \frac{\sum_{m=1}^M \sigma_{i,m}^2 \mathbf{c}_m}{\sum_{m=1}^M \sigma_{i,m}^2} - \mathbf{p}_{u,i} \quad (92)$$

is the error component introduced by the added noise. Thus, the localization error is simplified as

$$\tilde{\mathbf{p}}_{u,i} - \mathbf{p}_{u,i} \approx \frac{\Delta_g + \mu \Delta_n}{1 + \mu} \quad (93)$$

The proof is completed.

REFERENCES

- [1] Y. Zeng, J. Chen, J. Xu, D. Wu, X. Xu, S. Jin, X. Gao, D. Gesbert, S. Cui, and R. Zhang, "A tutorial on environment-aware communications via channel knowledge map for 6G," *IEEE Commun. Surv. Tutor.*, 2024.
- [2] C. He, Y. Dong, and Z. J. Wang, "Radio map assisted multi-UAV target searching," *IEEE Trans. on Wireless Commun.*, vol. 22, no. 7, pp. 4698–4711, 2023.
- [3] W. Chen and J. Chen, "Diffraction and scattering aware radio map and environment reconstruction using geometry model-assisted deep learning," *IEEE Trans. on Wireless Commun.*, 2024.
- [4] W. Liu and J. Chen, "UAV-aided radio map construction exploiting environment semantics," *IEEE Trans. on Wireless Commun.*, vol. 22, no. 9, pp. 6341–6355, 2023.
- [5] D. Wu, Y. Zeng, S. Jin, and R. Zhang, "Environment-aware hybrid beamforming by leveraging channel knowledge map," *IEEE Trans. on Wireless Commun.*, vol. 23, no. 5, pp. 4990–5005, 2024.
- [6] E. Moeen Taghavi, R. Hashemi, N. Rajatheva, and M. Latva-Aho, "Environment-aware joint active/passive beamforming for RIS-aided communications leveraging channel knowledge map," *IEEE Commun. Lett.*, vol. 27, no. 7, pp. 1824–1828, 2023.
- [7] N. Dal Fabbro, M. Rossi, G. Pillonetto, L. Schenato, and G. Piro, "Model-free radio map estimation in massive mimo systems via semi-parametric gaussian regression," *IEEE Trans. on Wireless Commun.*, vol. 11, no. 3, pp. 473–477, 2022.
- [8] D. Romero, P. Q. Viet, and R. Shrestha, "Aerial base station placement via propagation radio maps," *IEEE Trans. on Commun.*, vol. 72, no. 9, pp. 5349–5364, 2024.
- [9] Y. Zeng, X. Xu, S. Jin, and R. Zhang, "Simultaneous navigation and radio mapping for cellular-connected UAV with deep reinforcement learning," *IEEE Trans. on Wireless Commun.*, vol. 20, no. 7, pp. 4205–4220, 2021.
- [10] B. Li and J. Chen, "Radio map-assisted approach for interference-aware predictive UAV communications," *IEEE Trans. on Wireless Commun.*, vol. 23, no. 11, pp. 16 725–16 741, 2024.
- [11] S. Zhang and R. Zhang, "Radio map-based 3D path planning for cellular-connected UAV," vol. 20, no. 3, pp. 1975–1989, 2021.
- [12] S. Timilsina, S. Shrestha, and X. Fu, "Quantized radio map estimation using tensor and deep generative models," *IEEE Trans. Signal Process.*, vol. 72, pp. 173–189, 2024.
- [13] Y. Teganya and D. Romero, "Deep completion autoencoders for radio map estimation," *IEEE Trans. on Wireless Commun.*, vol. 21, no. 3, pp. 1710–1724, 2022.
- [14] O. Esrafilian, R. Gangula, and D. Gesbert, "Map reconstruction in UAV networks via fusion of radio and depth measurements," 2021, pp. 1–6.
- [15] Z. Chen, Z. Zhang, Z. Yang, and L. Liu, "Channel mapping based on interleaved learning with complex-domain MLP-mixer," *IEEE Wirel. Commun. Lett.*, vol. 13, no. 5, pp. 1369–1373, 2024.
- [16] H. Sun and J. Chen, "Propagation map reconstruction via interpolation assisted matrix completion," *IEEE Trans. Signal Process.*, vol. 70, pp. 6154–6169, 2022.
- [17] F. Pei, M. Shi, and Y. Xie, "Federated fingerprint localization method based on adaptive aggregation and feature alignment," *IEEE Wirel. Commun. Lett.*, vol. 14, no. 2, pp. 465–469, 2025.
- [18] Z. Wang, Y. Zhu, D. Wang, and Z. Han, "Secure trajectory publication in untrusted environments: A federated analytics approach," *IEEE Trans. Mob. Comput.*, vol. 22, no. 11, pp. 6742–6754, 2023.
- [19] T. Zhang, D. Xu, P. Ren, K. Yu, and M. Guizani, "Dflnet: Deep federated learning network with privacy preserving for vehicular lora nodes fingerprinting," *IEEE Trans. Veh. Technol.*, vol. 73, no. 2, pp. 2901–2905, 2024.
- [20] A. Islam, H. Karimipour, and A. O. Fapojuwo, "A federated meta learning-based secure data consolidation scheme for industrial aiot leveraging drone," *IEEE Trans. Veh. Technol.*, vol. 74, no. 1, pp. 1702–1707, 2025.
- [21] J. Tian, W. Chen, and J. Chen, "Differential privacy in federated learning for collaborative radio map construction and environment sensing," in *Proc. IEEE Int. Conf. Commun. Workshops*, 2024, pp. 792–797.
- [22] M. Al-Quraan, A. Zoha, A. Centeno, H. B. Salameh, S. Muhaidat, M. A. Imran, and L. Mohjazi, "Enhancing reliability in federated mmwave networks: A practical and scalable solution using radar-aided dynamic blockage recognition," *IEEE Trans. Mob. Comput.*, vol. 23, no. 10, pp. 10 146–10 160, 2024.
- [23] H. B. McMahan, E. Moore, D. Ramage, S. Hampson, and B. A. y. Arcas, "Communication-efficient learning of deep networks from decentralized data," *arXiv preprint arXiv:1602.05629*, 2017.
- [24] M. Yurochkin, M. Agarwal, S. Ghosh, K. Greenwald, N. Hoang, and Y. Khazaeni, "Bayesian nonparametric federated learning of neural networks," in *Proc. Int. Conf. Mach. Learn.*, 2019, pp. 7252–7261.
- [25] W. Chen and J. Chen, "Blockage-aware radio map construction via exploiting the diffraction and obstruction structure," in *Proc. IEEE Global Commun. Conf.*, 2023, pp. 1920–1925.
- [26] X. Li, K. Huang, W. Yang, S. Wang, and Z. Zhang, "On the convergence of fedavg on non-iid data," *arXiv preprint arXiv:1907.02189*, 2019.
- [27] K. Wei, J. Li, M. Ding, C. Ma, H. H. Yang, F. Farokhi, S. Jin, T. Q. Quek, and H. V. Poor, "Federated learning with differential privacy: Algorithms and performance analysis," *IEEE Trans. Inf. Forensics Secur.*, vol. 15, pp. 3454–3469, 2020.